RSC Advances

ROYAL SOCIETY OF CHEMISTRY

www.rsc.org/advances

Journal Name

RSCPublishing

Article

Nanocomposite $Li_3V_2(PO_4)_3$/Carbon as a cathode material with high rate performance and long-term cycling stability in lithium-ion batteries

Peixun Xiong,[a,b] Lingxing Zeng, [a,b] Huan Li, [a,b] Cheng Zheng, [a,b] Mingdeng Wei*[a,b]

Cite this: DOI: 10.1039/xoxxoooooox

Received ooth January 2015,
Accepted ooth January 2015

DOI: 10.1039/xoxxoooooox

www.rsc.org/

In the present work, nanocomposite $Li_3V_2(PO_4)_3$/Carbon is successfully synthesized by combining sol-gel method and nanocasting route, and then is characterized by means of X-ray diffraction (XRD), thermogravimetric analysis (TG), N_2 adsorption-desorption, transmission electron microscopy (TEM). Furthermore, this nanocomposite is used as a cathode material for Li-ion intercalation and exhibits large reversible capacity, high rate performance and excellent long-term cycling stability. For instance, a large reversible capacity of 95 mAh g^{-1} and an average Coulombic efficiency of 99.1% can be maintained even after 3000 cycles at a high rate of 20 C in the potential range of 3.0-4.3 V. Moreover, the $Li_3V_2(PO_4)_3$/C nanocomposite delivered a large capacity of 127 mAh g^{-1} at a high rate of 10 C in the voltage range of 3.0-4.8 V. The super results might be attributed to the unique hierarchical architecture of the $Li_3V_2(PO_4)_3$/Carbon nanocomposite.

Introduction

With increasing concerns regarding environmental protection and global warming, there is a strong and increasing demand for the development of power sources for hybrid electric vehicles (HEVs) and renewable energy systems.[1] The lithium-ion batteries (LIBs) have widely been applied as clean and renewable power source for the portable electronic devices such as digital video, notebook PCs, and have also been proposed for use in electric vehicles and large-scale energy storage.[2-5] However, the performance of current LIBs cannot meet the requirements of electric vehicles in terms of high rate performance and long term cycling stability.[6-13]

Recently, $Li_3V_2(PO_4)_3$ has been identified as a promising candidate cathode material for LIBs due to its good ion mobility, high theoretical capacity and high operating voltage.[14-21] Despite these advantages, $Li_3V_2(PO_4)_3$ still suffers from the problem of poor capacity and cycling stability at high rate because of its low electronic conductivity as well as the side reaction between the active material and organic electrolyte. It is well known that small particle size, carbon coating, and doping of other metal ions are beneficial for improving the electrochemical properties of $Li_3V_2(PO_4)_3$.[22] Among various approaches, carbon coating plays an important role due to the advantages arising from the unique properties of carbon, such as unique physical properties, chemical and electrochemical stability.[23-27] Moreover, nano-size provides a shorter path for Li-ion and electron transport, which facilitates improved kinetics.[28-33] However, the preparation of a $Li_3V_2(PO_4)_3$/Carbon composite ($Li_3V_2(PO_4)_3$/C) with nano-size is not an easy issue. The formation of a $Li_3V_2(PO_4)_3$ phase with an electrical conductive carbon layer generally involves high sintering temperature and long sintering time, in which $Li_3V_2(PO_4)_3$ tends to grow and aggregate into large grains.

In recent studies, mesoporous carbon (MC) has been used as a promising nanoreactor for fabricating nanomaterials with high Li-ion storage capability and stability.[34-39] The mesochannel and large surface area of MC shortens the distance of Li-ion diffusion and its high conductivity is in favor to electron transmission. On the other hand, it has large pore volumes, which offer a better accommodation of the strain and volume changes during the charge-discharge process. These results encouraged us to extend our studies to the investigation of nanocomposite composed of mesoporous carbon and $Li_3V_2(PO_4)_3$. In the present work, the nanocomposite $Li_3V_2(PO_4)_3$/C was synthesized by combining sol-gel method and nanocasting route, and exhibited excellent rate performance and long-term cycling stability for Li-ion intercalation. Furthermore, the relationships between the intrinsic of nanocomposite $Li_3V_2(PO_4)_3$/C and the electrochemical properties were also investigated in detail.

Experimental

1. Preparation and characterizations

The synthesis process of mesoporous carbon is similar to that described by Ryoo.[40-41] For a typical synthesis of $Li_3V_2(PO_4)_3$/C nanocomposite, 0.244 g of Li_2CO_3, 0.759 g of $NH_4H_2PO_4$, 0.515g NH_4VO_3 and 0.1 g citric acid were dispersed in 20 mL of hot distilled water under ultrasonication for 0.5 h to form a bright yellow solution. Then 0.1 g of MC powder was introduced to the solution, under ultrasonication

for 30 min. Then the mixture was vigorous stirring for 12 h at 40 °C. After the obtained mixture was heated at 75 °C for 1h, it was ground and then calcined at 700 °C in Ar for 5 h to obtain the $Li_3V_2(PO_4)_3$/C nanocomposite sample.

XRD patterns were recorded on a PANalytical X'Pert spectrometer using the Co Kα radiation (λ= 1.789 Å), and the data would be changed to Cu Kα data. SEM and TEM were taken on a Hitachi 4800 instrument and a FEI F20 S-TWIN instrument, respectively. N_2 adsorption–desorption analysis was measured on a Micromeritics ASAP 2020 instrument, pore volumes were determined using the adsorbed volume at a relative pressure of 0.99, multipoint Brunauer-Emmet-Teller (BET) surface area was estimated from the relative pressure range from 0.06 to 0.3. To determine the actual amount of carbon in the nanocomposites, thermogravimetric analysis (TGA) was performed using a CHNS/O analyzer (PE 2400II, Perkin Elmer, America) in air atmosphere.

2. Electrochemical measurements

For the electrochemical measurement, 80 wt% active materials ($Li_3V_2(PO_4)_3$/C nanocomposite) was mixed and grounded with 10 wt% polyvinylidene fluoride (PVDF) powder as a binder and 10 wt% acetylene back carbon (AB) powder as the conductive assistant materials. The mixture was spread and pressed on Al foil circular flakes as the working electrode (WE), and dried at 120 ºC for 12 h under the vacuum conditions. Metallic lithium foils were used as the negative electrodes. The electrolyte was 1M $LiPF_6$ in a 1/1/1 (volume ratio) mixture of ethylene carbonate (EC), ethylene methyl carbonate (EMC) and dimethyl carbonate (DMC). The separator was UP 3093 (Japan) micro-porous polypropylene membrane. The specific capacity values of $Li_3V_2(PO_4)_3$/C nanocomposite are calculated on the basis of the mass of $Li_3V_2(PO_4)_3$. In average, the amount of active material in test cells was ca. 1 - 2 mg. Without any specific explanation, the galvanostatic charge and discharge experiment was performed in the range of 3.0 - 4.3 V (1 C =133 mAh g^{-1}) and 3.0-4.8 V (1 C =198 mAh g^{-1}) (vs. Li^+/Li) at room temperature, respectively. The cells were assembled in a glove box filled with highly pure argon gas (O_2 and H_2O levels < 1 ppm), and charge/discharge tests were performed on a Land automatic batteries tester (Land CT 2001A, Wuhan, China).

Results and discussion

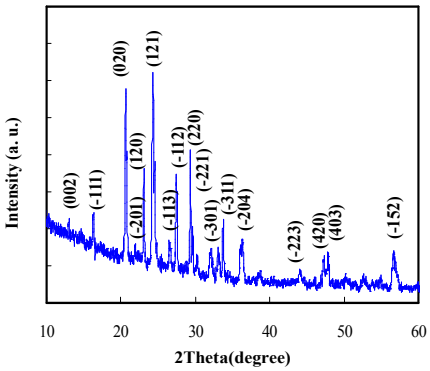

Fig. 1 XRD patterns of $Li_3V_2(PO_4)_3$/C nanocomposite.

Fig. 1 shows the XRD pattern of $Li_3V_2(PO_4)_3$/C nanocomposite. As seen from **Fig. 1**, all diffraction peaks can be ascribed to the characteristic peaks of monoclinic $Li_3V_2(PO_4)_3$ (JCPDS 080-1515), confirming that $Li_3V_2(PO_4)_3$/C nanocomposite can be obtained. The citric acid can promote raw materials to reach atomic level mixing and homogenously trap around the mesoporous carbon channels, which reduces particle size to nanoscale level. Apart from reducing metal oxide during the reaction process, mesoporous carbon can be involved in controlling the particle growth and providing a conductive network to facilitate electron transfer, and as a result, the electrode performances could be enhanced. Based on N_2 adsorption-desorption analysis, it was found that the BET surface area and pore volume were 134 m^2 g^{-1} and 0.22 cm^3 g^{-1} for $Li_3V_2(PO_4)_3$/C nanocomposite.

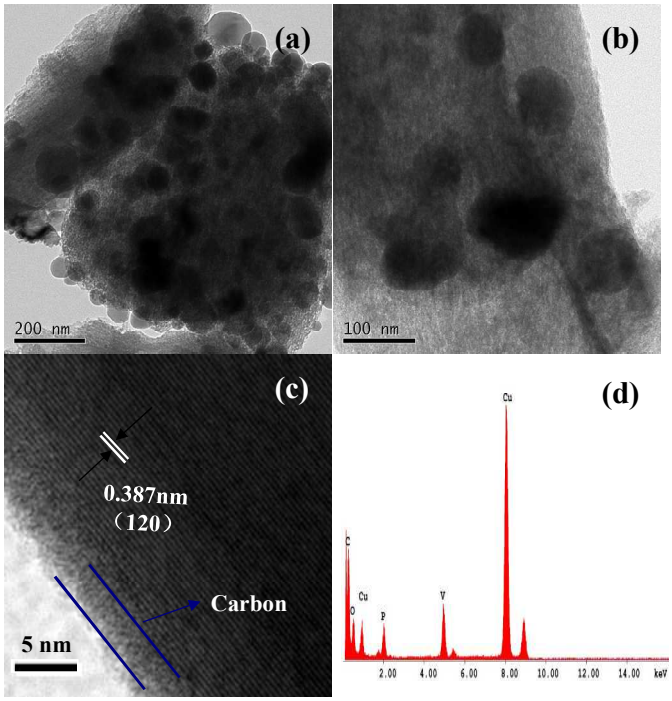

Fig. 2 (a-b) TEM images of $Li_3V_2(PO_4)_3$/C nanocomposite; (c) HRTEM images of $Li_3V_2(PO_4)_3$/C nanocomposite; (d) EDS spectra obtained from (b) $Li_3V_2(PO_4)_3$/C nanocomposite.

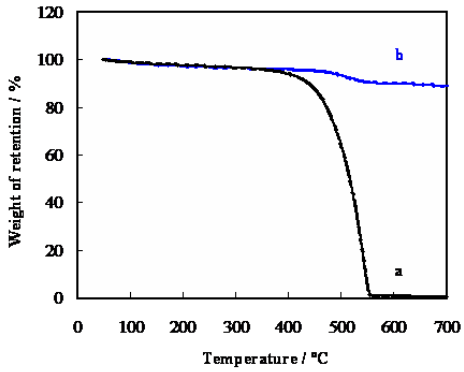

Fig. 3 TGA curves of (a) MC and (b) $Li_3V_2(PO_4)_3$/C nanocomposite.

TEM images of $Li_3V_2(PO_4)_3$/C nanocomposite are presented in **Fig. 2.** As shown in **Fig. 2a-b**, most of $Li_3V_2(PO_4)_3$ nanoparticles were partially loaded inside and outside channels of mesoporous carbon matrix in the $Li_3V_2(PO_4)_3$/C nanocomposite. It can also be found that the size of

$Li_3V_2(PO_4)_3$ nanoparticles in the nanocomposite ranged from 30 to 80 nm, **Fig. 2c** shows the HRTEM images of $Li_3V_2(PO_4)_3$/C nanocomposite. A thin coating layer of carbon was formed on the surface of particles and its thickness was estimated to be ca. 2–3 nm. It also showed that these nanoparticles were high crystalline and the lattice fringe was found to be approximately 0.387 nm, corresponding to the d_{120}-spacing of monoclinic $Li_3V_2(PO_4)_3$. The chemical composition of the $Li_3V_2(PO_4)_3$/C nanocomposite were measured by EDS, as depicted in **Fig. 2d**. It was also confirmed that the sample existed carbon, oxygen, phosphorus and vanadium elements. The Li element cannot be detected because of the detection limit of EDS. The presence of oxygen mainly came from $Li_3V_2(PO_4)_3$, and a little from atmospheric O_2, or CO_2 adsorbed on the surface of the sample.

To confirm the amount of carbon in $Li_3V_2(PO_4)_3$/C nanocomposite, TGA was carried out in air and the result is depicted in **Fig.3**. The samples were heated from 50 to 700 °C at a rate of 5 °C min^{-1}. The weight loss below 150 °C was probably due to the evaporation of adsorbed moisture, considering the relatively high surface area of the samples. As can be seen from **Fig. 3a**, the maximum weight loss of MC samples was taken place at 400-550 °C. According to **Fig. 3b**, the content of carbon was estimated to be ca. 11.5 wt% for the $Li_3V_2(PO_4)_3$/C nanocomposite.

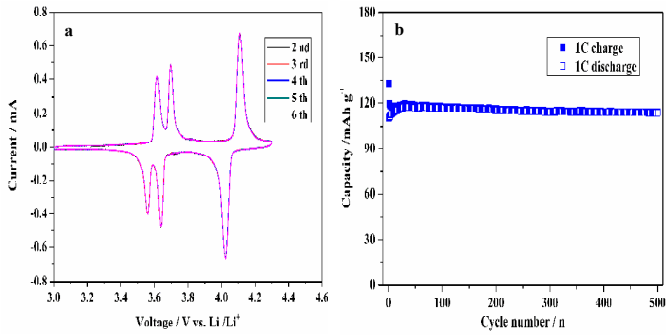

Fig. 4 (a) CV of $Li_3V_2(PO_4)_3$/C nanocomposite at a scan rate of 0.5 mV s^{-1} between 3.0-4.3 V; (b) The cycling performance of $Li_3V_2(PO_4)_3$/C nanocomposite electrode at 1 C in a potential range of 3.0-4.3 V (1C =133 mAh g^{-1}).

The electrochemical behavior of $Li_3V_2(PO_4)_3$-C nanocomposite electrode was measured by CV at a scanning rate of 0.5 mV s^{-1} between 3.0 and 4.3 V. As depicted in **Fig. 4a**, the peaks of $Li_3V_2(PO_4)_3$/C nanocomposite are sharp and have a high intensity. The well-defined anodic and cathodic peaks were observed at around 3.57/3.59, 3.65/3.67 and 4.04/4.07 V. Monoclinic $Li_3V_2(PO_4)_3$ contains three independent lithium sites. Such three pairs of charge/discharge plateaus were associated with two Li^+ insertion/extraction into/out of the monoclinic $Li_3V_2(PO_4)_3$ lattice based on the V^{3+}/V^{4+} redox couple, respectively. The Li^+ insertion/extraction into/out of $Li_3V_2(PO_4)_3$ can be written as the following equtions.[5, 42-43]

$$Li_3V_2(PO_4)_3 \leftrightarrow Li_{2.5}V_2(PO_4)_3 + 0.5Li^+ + 0.5e^- \quad (1)$$

$$Li_{2.5}V_2(PO_4)_3 \leftrightarrow Li_2V_2(PO_4)_3 + 0.5Li^+ + 0.5e^- \quad (2)$$

$$Li_2V_2(PO_4)_3 \leftrightarrow LiV_2(PO_4)_3 + Li^+ + e^- \quad (3)$$

The potential difference between the anodic peaks and the corresponding cathodic peaks is small in $Li_3V_2(PO_4)_3$/C nanocomposite, indicating an alleviated polarization and facile extraction/insertion of Li^+ in $Li_3V_2(PO_4)_3$/C nanocomposite. Moreover, the second and sixth CV curves remained steady, indicating the highly reversible performance of $Li_3V_2(PO_4)_3$/C nanocomposite electrode.

Fig. 4b shows the cycling performances of $Li_3V_2(PO_4)_3$/C nanocomposite at a current rate of 1 C in a potential window of 3.0-4.3 V (1C =133 mAh g^{-1}). It exhibits an initial discharge capacity of 110 mAh g^{-1} and the charge capacity of 132 mAh g^{-1}, corresponding to a Coulombic efficiency of 83.3%, which is relatively higher than previous $Li_3V_2(PO_4)_3$-based materials.[21] The Coulombic efficiency of the $Li_3V_2(PO_4)_3$/C nanocomposite was up to 98.9% after the initial 10 cycles. As can be found that the cathode made of $Li_3V_2(PO_4)_3$/C nanocomposite exhibited the discharge capacities of 116.1, 115.3, 114.4, 114 and 113.8 mAh g^{-1} for the 100 th, 200 th, 300 th, 400 th, 500 th cycle, respectively. It is surprising to note that there was less capacity loss even after 500 cycles, which is better than other $Li_3V_2(PO_4)_3$-based materials.[44]

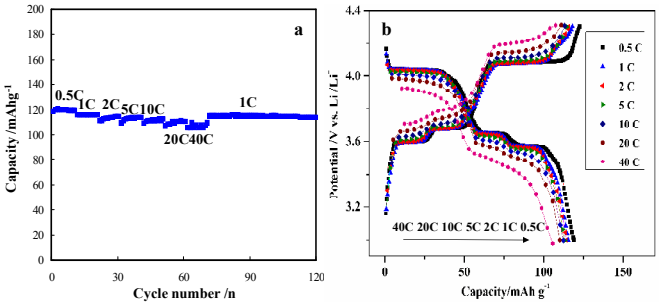

Fig. 5 (a) The rate capacity and (b) charge-discharge curves of $Li_3V_2(PO_4)_3$/C nanocomposite in a potential range of 3.0-4.3 V.

Fig. 5a presents the rate capability of the $Li_3V_2(PO_4)_3$/C nanocomposite from 0.5 to 40 C for 10 cycles at each current rate. This material keeps a slightly increasing reversible capacity after each 10 th cycle at a high current rate. As can be seen, the $Li_3V_2(PO_4)_3$/C nanocomposite delivered the high discharge capacities of 118, 115, 114, 113, 112 and 110 mA h g^{-1} at current rates of 0.5, 1, 2, 5, 10 and 20 C, respectively. Remarkably, the $Li_3V_2(PO_4)_3$/C nanocomposite had a stable capacity of 106 mA h g^{-1} even at a current rate as high as 40 C, indicating that such a material deliver a high-rate performance. It is noteworthy that the capacity can be restored to its original state even if the current density was returned to 1 C after this high-rate measurement. **Fig. 5b** displays galvanostatic charge-discharge voltage profiles of the $Li_3V_2(PO_4)_3$/C nanocomposite measured at a gradually increased current rate in a potential range of 3.0-4.3 V. The curves for $Li_3V_2(PO_4)_3$/C nanocomposite exhibit three charge-discharge plateaus, which identified as the two-phase transition processes during electrochemical reactions of $Li_3V_2(PO_4)_3$, which agrees well with the CV curves depicted in **Fig. 4a**. With the increase in charge/discharge current density, $Li_3V_2(PO_4)_3$/C nanocomposite exhibited excellent cycling stability at both high and low current rate. It can be found that the charge/discharge plateaus at a high current rate of 40 C are apparent, indicating that $Li_3V_2(PO_4)_3$/C nanocomposite had super high rate performance. It is obvious that the $Li_3V_2(PO_4)_3$ nanocomposite has a small voltage difference of the charge-discharge plateaus and high

specific capacities, indicating that $Li_3V_2(PO_4)_3$/C nanocomposite has low electrochemical polarization.[45-46] In a word, $Li_3V_2(PO_4)_3$/C nanocomposite exhibited the high capacity and excellent rate capability.

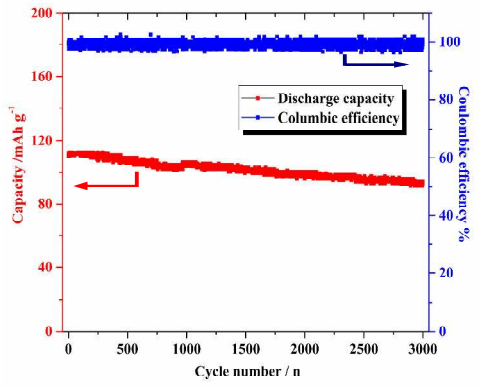

Fig. 6 The long-term cycling performance and Coulombic efficiency of $Li_3V_2(PO_4)_3$/C nanocomposite at a current rate of 20 C in a potential range of 3.0-4.3 V.

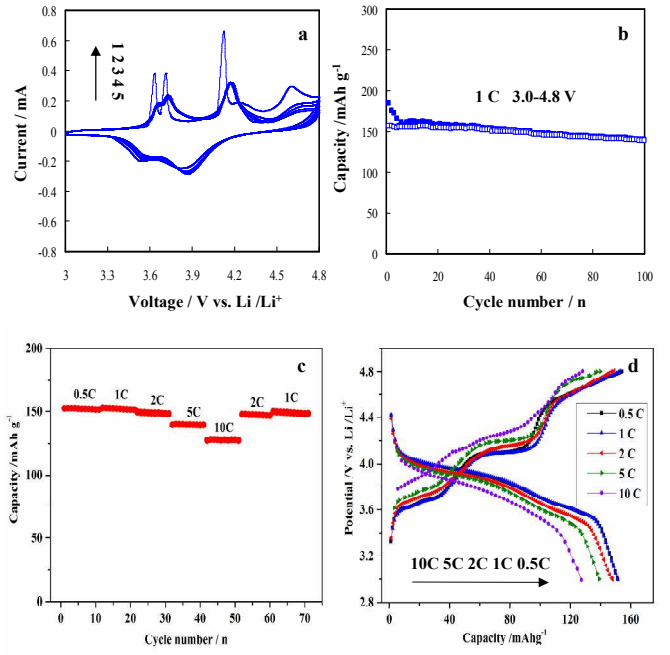

Fig. 7 Electrochemical performance of $Li_3V_2(PO_4)_3$/C nanocomposite in the potential range of 3.0-4.8 V (1C =198 mAh g^{-1}) for lithium ion batteries. (a) CV curves at a scan rate of 0.5 mV s^{-1}, (b) The cycling performance at 1 C, (c) The rate capacity, and (d) charge–discharge curves of $Li_3V_2(PO_4)_3$/C nanocomposite at different current rates between 0.5 and 10 C.

In order to investigate the long-term cycling stability at high rate, we increased the charge/discharge rate to 20 C. **Fig. 6** shows the long-term cycling performance and Coulombic efficiency of $Li_3V_2(PO_4)_3$/C nanocomposite at a high rate of 20 C in a potential range of 3.0-4.3 V. The electrode was cycled at 0.5 C for initial 5 cycles and then turned to 20 C. As shown in **Fig. 6**, this material maintained a high Coulombic efficiency, with an average value of 99.1% over 3000 cycles. After 1000 cycles, the electrode retained a high capacity of 105.6 mAh g^{-1} at a high rate of 20 C, and maintained as high as 95.9% of its initial reversible capacity (only 4.1% total capacity loss; ~0.004% per cycle). Even after 3000 cycles, the $Li_3V_2(PO_4)_3$/C nanocomposite electrode still retained the capacity of 95.1 mA h g^{-1}. An average specific discharge capacity in 3000 cycles at 20 C was about 101.8 mAh g^{-1}. The specific capacity and long-term cycling stability for $Li_3V_2(PO_4)_3$/C nanocomposite cathode are better than most of previous reported $Li_3V_2(PO_4)_3$-based cathodes.[24, 47-49]

The electrochemical performance of $Li_3V_2(PO_4)_3$/C nanocomposite was test in the potential range of 3.0-4.8 V (1C =198 mAh g^{-1}) for LIBs. **Fig. 7a** presents the CV curves of $Li_3V_2(PO_4)_3$/C nanocomposite at a scan rate of 0.5 mV s^{-1} between 3.0 and 4.8 V. As depicted in **Fig. 7a**, there are four sharp and well-shaped anodic peaks in the first charge curve, corresponding to a sequence of phase transition processes of $Li_3V_2(PO_4)_3 \rightarrow Li_{2.5}V_2(PO_4)_3 \rightarrow Li_2V_2(PO_4)_3 \rightarrow LiV_2(PO_4)_3 \rightarrow V_2(PO_4)_3$. When charged up to 4.8 V, the extraction of the third Li^+ will take place. Obviously, the anodic peak current at 4.6 V is the lowest, which is ascribed to the fact that it is difficult to extract the third Li^+ in the monoclinic $Li_3V_2(PO_4)_3$. The second and fifth CV curves remained overlapped, indicating the highly reversible performance of $Li_3V_2(PO_4)_3$/C nanocomposite. **Fig. 7b** shows the cycling performances of $Li_3V_2(PO_4)_3$/C nanocomposite at a current rate of 1 C in a potential window of 3.0-4.8 V (1C =198 mAh g^{-1}). It can be found that the cathode made of $Li_3V_2(PO_4)_3$/C nanocomposite exhibited the discharge capacities of 156.8, 155.1, 149.3 and 139.8 mAh g^{-1} for the 2 nd, 5 th, 50 th, 100 th cycle, respectively. After 100 cycles, the electrode retained a high capacity of 139.8 mAh g^{-1} at 1 C and maintained 89% of its initial reversible capacity, which is better than those of previous results.[18, 44, 49] **Fig. 7c-d** depict the rate capacity and charge–discharge curves of $Li_3V_2(PO_4)_3$/C nanocomposite in a potential range of 3.0-4.8 V at different current rates between 0.5 and 10 C. This material delivered high discharge capacities of 152, 151, 148, 139 and 127 mAh g^{-1} at 0.5, 1, 2, 5 and 10 C, respectively. It is noteworthy that the capacity can be restored to its original state even if the current density was returned to 1 C. With increasing current rates, the charge-discharge plateaus became shorter, and the difference in potential between the charging and discharging plateaus increased gradually. However, the charge/discharge plateaus at a high current rate of 10 C are apparent, indicating that $Li_3V_2(PO_4)_3$/C nanocomposite has a high rate performance in the potential of 3.0-4.8 V.

The cathode material made of $Li_3V_2(PO_4)_3$/C nanocomposite shows large capacity, high rate performance and excellent long-term cycling stability, which is probably originate from the unique hierarchical architecture. The Li-ions and electrolyte are readily transported in the mesoporous carbon matrix and electrons transport rapidly through the thin carbon layer on the surface of $Li_3V_2(PO_4)_3$ nanoparticles. Such a structure led to a significantly increased electrical conductivity of the overall electrode, resulting in a reduction in the cathode polarization. Moreover, the addition of mesoporous carbon and citric acid led to the small particle size and high degree of crystallinity of $Li_3V_2(PO_4)_3$ during the sintering process, which provides fast Li-ion and electron transport as well as large active surface area. Therefore, the cell made of $Li_3V_2(PO_4)_3$/C nanocomposite can achieve excellent long-term cycling stability, large capacity and high rate capability.

Conclusions

In summary, nanocomposite $Li_3V_2(PO_4)_3$/C was successfully synthesized by combining sol-gel method and nanocasting route. It was found that the size of synthesized particles was only 30-80 nm, which was coated by a thin carbon layer. The $Li_3V_2(PO_4)_3$/C nanocomposite was used as a cathode material in the rechargeable LIBs and exhibited large reversible capacity, high rate performance and excellent long-term cycling stability. For instance, a large reversible capacity of 95 mAh g^{-1} and an average Coulombic efficiency of 99.1% can be maintained even after 3000 cycles at high rate of 20 C in the potential range of 3.0-4.3 V. Moreover, the $Li_3V_2(PO_4)_3$/C nanocomposite delivered a large capacity of 127 mAh g^{-1} at a high rate of 10 C in the voltage range of 3.0-4.8 V. Such excellent properties might be attributed to the unique hierarchical architecture of the $Li_3V_2(PO_4)_3$/C nanocomposite.

Acknowledgements

This work was financially supported by National Natural Science Foundation of China (NSFC 21173049).

Notes and references

[a] State Key Laboratory of Photocatalysis on Energy and Environment, Fuzhou University, Fuzhou, Fujian 350002, China.

[b] Institute of Advanced Energy Materials, Fuzhou University, Fuzhou, Fujian 350002, China. E-mail: wei-mingdeng@fzu.edu.cn; Tel: +86-591-83753180

1 M. Armand and J.-M. Tarascon, *Nature*, 2008, **451**, 652-657.

2 M. V. Reddy, G. V. Subba Rao and B. V. R. Chowdari, *Chem. Rev.*, 2013, **113**, 5364-5457.

3 Y. L. Liang, Z. L. Tao and J. Chen, *Adv. Energy Mater.*, 2012, **2**, 742-769.

4 A. K. Padhi, K. S. Nanjndaswamy and J. B. Goodenough, *J. Electrochem. Soc.*, 1997, **144**, 1188-1194.

5 S. C. Yin, H. Grondey, P. Strobel, M. Anne and L. F. Nazar, *J. Am. Chem. Soc.*, 2003, **125**, 10402-10411.

6 X. Sen, Y. G. Guo and L. J. Wan, *Acc. Chem. Res.*, 2012, **45**, 1759-1769.

7 H. J. Yu and H. S. Zhou, *J. Phys. Chem. Lett.*, 2013, **4**, 1268-1280.

8 Y. S. Hu, Y. G. Guo, R. Dominko, M. Gaberscek, J. Jamnik and J. Maier, *Adv. Mater.*, 2007, **19**, 1963-1966.

9 Y. G. Wang, Y. R. Wang, E. Hosono, K. X. Wang and H. S. Zhou, *Angew. Chem. Int. Ed.*, 2008, **47**, 7461-7465.

10 I. Moriguchi, R. Hidaka, H. Yamada, T. Kudo, H. Murakami and N. Nakashima, *Adv. Mater.*, 2006, **18**, 69-73.

11 J. Li, C. Yue, Y. J. Yu, Y. S. Chui, J. Yin, Z. G. Wu, C. D. Wang, Y. S. Zang, W. Lin, J. T. Li, S. T. Wu and Q. H. Wu, *J. Mater. Chem. A*, 2013, **1**, 14344-14349.

12 P. J. Zhang, L. B. Wang, J. Xie, L. W. Su and C. A. Ma, *J. Mater. Chem. A*, 2014, **2**, 3776-3782.

13 L. X. Zeng, C. Zheng, L. C. Xia, Y. X. Wang and M. D. Wei, *J. Mater. Chem. A*, 2013, **1**, 4293-4299.

14 X. H. Rui, Q. Y. Yan, M. S. Kazacos and T. M. Lim, *J. Power Sources*, 2014, **258**, 19-38.

15 C. Wang, Z. Y. Guo, W. Shen, Q. J. Xu, H. M. Liu and Y. G. Wang, *Adv. Funct. Mater.*, 2014, **21**, 5511-5521.

16 M. M. Ren, Z. Zhou, Y. Z. Li, X. P. Gao and J. Yan, *J. Power Sources*, 2006, **162**, 1357-1362.

17 M. M. Ren, Z. Zhou, L. W. Su and X. P. Gao, *J. Power Sources*, 2009, **189**, 786-789.

18 H. D. Liu, P. Gao, J. H. Fang and G. Yang, *Chem. Commun.*, 2011, **47**, 9110-9112.

19 A. Q. Pan, J. Liu, J. G. Zhang, W. Xu, G. Z. Cao, Z. M. Nie, B. W. Arey and S. Q. Liang, *Electrochem. Commun.*, 2010, **12**, 1674-1677.

20 X. H. Rui, D. H. Sim, K. M. Wong, J. X. Zhu, W. L. Liu, C. Xu, H. T. Tan, N. Xiao, H. H. Hng, T. M. Lim and Q. Y. Yan, *J. Power Sources*, 2012, **214**, 171-177.

21 X. P. Zhang, H. J. Guo, X. H. Li, Z. X. Wang and L. Wu, *Electrochim. Acta*, 2012, **64**, 65-70.

22 C. W. Sun, S. Rajasekhara, Y. Z. Dong and J. B. Goodenough, *ACS Appl. Mater. Interfaces*, 2011, **3**, 3772-3776.

23 G. X. Wang, H. Liu, J. Liu, S. Z. Qiao, G. Q. Lu, P. Munro and H. Ahn, *Adv. Mater.*, 2010, **22**, 4944-4948.

24 S. L. Wang, Z. X. Zhang, Z. T. Jiang, A. Deb, L. Yang and S.-I. Hirano, *J. Power Sources*, 2014, **253**, 294-299.

25 X. F. Zhang, K. X. Wang, X. Wei and J. S. Chen, *Chem. Mater.*, 2011, **23**, 5290-5292.

26 J. Z. Chen, L. Yang, S. H. Fang and S.-I. Hirano, *Electrochem. Commun.*, 2011, **13**, 848-851.

27 L. X. Zeng, C. Zheng, J. C. Xi, H. L. Fei and M. D. Wei, *Carbon*, 2013, **62**, 382-388.

28 C. B. Zhu, Y. Yu, L. Gu, K. Weichert and J. Maier, *Angew. Chem. Int. Ed.*, 2011, **50**, 6278-6282.

29 J. S. Chen, Y. L. Tan, C. M. Li, Y. L. Cheah, D. Y. Luan, S. Madhavi, F. Y. C. Boey, L. A. Archer and X. W. Lou, *J. Am. Chem. Soc.*, 2010, **132**, 6124-6130.

30 L. Q. Mai, S. Li, Y. F. Dong, Y. L. Zhao, Y. Z. Luo and H. M. Xu, *Nanoscale*, 2013, **5**, 4864-4869.

31 A. Q. Pan, D. W. Choi, J. G. Zhang, S. Q. Liang, G. Z. Cao, Z. M. Nie, B. W. Arey and J. Liu, *J. Power Sources*, 2011, **196**, 3646-3649.

32 D. L. Li, M. Tian, R. Xie, Q. Li, X. Y. Fan, L. Gou, P. Zhao, S. L. Ma, Y. X. Shi and H. T. H. Yong, *Nanoscale*, 2014, **6**, 3302-3308.

33 L. X. Zeng, C. Zheng, C. L. Deng, X. K. Ding and M. D. Wei, *ACS Appl. Mater. Interfaces*, 2013, **5**, 2182-2187.

34 X. Ji, K. T. Lee and L. F. Nazar. *Nat. Mater.*, 2009, **8**, 500-506.

35 H. S. Zhou, S. M. Zhu, M. Hibino, I. Honma and M. Ichihara, *Adv. Mater.*, 2003, **15**, 2107-2111.

36 L. F. Shen, E. Uchaker, C. Z. Yuan, P. Nie, M. Zhang, X. G. Zhang and G. Z. Cao, *ACS Appl. Mater. Interfaces*, 2012, **4**, 2985-2992.

37 F. Han, W. C. Li, M. R. Li and A. H. Lu, *J. Mater. Chem.*, 2012, **22**, 9645-9651.

38 L. X. Zeng, F. Y. Xiao, J. C. Wang, S. K. Gao, X. K. Ding and M. D. Wei, *J. Mater. Chem.*, 2012, **22**, 14284-14288.

39 A. L. Chen, C. X. Li, R. Tang, L. W. Yin and Y. X. Qi, *Phys. Chem. Chem. Phys.*, 2013, **15**, 13601-13610.

40 S. Jun, S. H. Joo, R. Ryoo, M. Kruk, M. Jaroniec, Z. Liu, T. Ohsuna and O. Terasaki, *J. Am. Chem. Soc.*, 2000, **122**, 10712-10713.

41 L. X. Zeng, Q. F. Li, G. N. Chen, D. P. Tang and M. D. Wei, *Electrochim. Acta*, 2012, **68**, 158-165.

42 W. C. Duan, Z. Hu, K. Zhang, F. Y. Cheng, Z. L. Tao and J. Chen, *Nanoscale*, 2013, **5**, 6485-6490.

43 C. Wang, H. M. Liu and W. S. Yang, *J. Mater. Chem.*, 2012, **22**, 5281-5285.
44 F. Teng, Z. H. Hu, X. H. Ma, L. C. Zhang, C. X. Ding, Y. Yu and C. H. Chen, *Electrochim. Acta*, 2013, **91**, 43-49.
45 J. Su, X. L. Wu, J. S. Lee, J. Kim and Y. G. Guo, *J. Mater. Chem. A*, 2013, **1**, 2508-2514.
46 L. Zhang, H. F. Xiang, Z. Li and H. H. Wang, *J. Power Sources*, 2012, **203**, 121-125.
47 Q. L. Wei, Q. Y. An, D. D. Chen, L. Q. Mai, S. Y. Chen, Y. L. Zhao, K. M. Hercule, L. Xu, A. M. Khan and Q. J. Zhang, *Nano Lett.*, 2014, **14**, 1042-1048.
48 Y. Q. Qiao, X. L. Wang, Y. J. Mai, J. Y. Xiang, D. Zhang, C. D. Gu and J. P. Tu, *J. Power Sources*, 2011, **196**, 8706-8709.
49 J. T. Xu, S. L. Chou, C. F. Zhou, Q. F. Gu, H. K. Liu and S. X. Dou, *J. Power Sources*, 2014, **246**, 124-131.

TOC

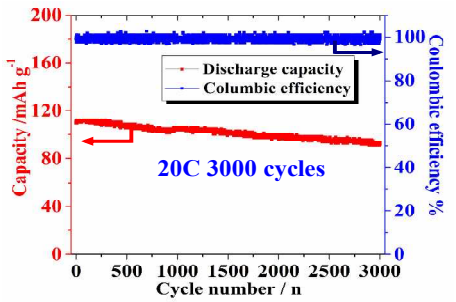

$Li_3V_2(PO_4)_3$/Carbon nanocomposite with high electrochemical performance has been successfully synthesized by combining sol-gel method and nanocasting route.